

Article

Growth and Thermal Properties of Mg-Doped Lithium Isotope Niobate ($\text{Mg}^{7}\text{LiNbO}_3$) Crystal

Nana Zhang ^{1,*}, Xishi Tai ¹ , Xiaoru Pan ¹, Mingjun Song ¹ and Jiyang Wang ²¹ College of Chemistry & Chemical and Environmental Engineering, Weifang University,

Weifang 261061, China; taixs@wfu.edu.cn (X.T.); sdwfyypxr@163.com (X.P.); smj521209@126.com (M.S.)

² State Key Laboratory of Crystal Materials, Shandong University, Jinan 250100, China; jywang@sdu.edu.cn

* Correspondence: zhangnana0801@wfu.edu.cn

Received: 10 July 2018; Accepted: 1 August 2018; Published: 3 August 2018



Abstract: An Mg-doped isotope lithium niobate ($\text{Mg}^{7}\text{LiNbO}_3$) crystal was successfully grown from ${}^7\text{LiOH}$, Nb_2O_5 , and MgO using the Crozchralski method. The weight of the as-grown crystal with good quality was about 40 g. The crystal structure was determined as an R_{3c} space group using the X-ray powder diffraction (XRPD) method, and the crystal composition (Li%) determined using the Raman mode linewidth method was 49.29%. The average transmittance of the crystal in the range of 500–2500 nm was approximately 72%. Various thermal properties, including the specific heat (C_p), the thermal expansion coefficient (α), the thermal diffusion coefficient (λ), and the thermal conductivity (κ), were carefully determined and calculated, and the value divergences among $\text{Mg}^{7}\text{LiNbO}_3$, the undoped isotope lithium niobate (${}^7\text{LiNbO}_3$), and natural lithium niobate (LiNbO_3) crystals were mainly related to the differences in microstructure caused by the crystal composition.

Keywords: single-crystal growth; isotope lithium niobite; thermal properties; neutron scattering

1. Introduction

Lithium niobate (LiNbO_3) crystals are multi-functional materials, which exhibit good photoelectric and piezoelectric properties, among others, and they are currently employed in many commercial applications [1–5]. Conventionally, a large size of good-quality LiNbO_3 crystals can be readily grown from Li_2CO_3 and Nb_2O_5 raw materials, whereby the crystals obtained are non-stoichiometric compounds (where $[\text{Li}]/[\text{Nb}] < 1$) [6]. The intrinsic defects of Li greatly influence the properties of these materials and limits their application. Therefore, it is significant to investigate the defect structure of LiNbO_3 crystals and explore the relationships between the structure and the properties of this material.

Several efforts were made to understand the intrinsic lattice characteristics of LiNbO_3 crystals, while there still remains some controversy surrounding its defect structure [7–17]. The X-ray diffraction technique is the primary method used to resolve crystal structure, whereas its drawbacks involve its insensitivity to light elements. For LiNbO_3 crystals, there exists Li and O light elements; thus, compared to X-ray techniques, neutron scattering is more sensitive to these light elements. In addition, the nuclear neutron scattering lengths of Li (−1.900 fm) and Nb (7.054 fm) are of the same order with an opposite sign. Taken together, these factors suggest that neutron scattering is a more powerful method than X-ray diffraction for resolving the LiNbO_3 crystal structure. However, the natural LiNbO_3 crystal is not suitable for further investigation on the crystal micro-structure using neutron scattering, as the natural Li element contains two isotopes of ${}^6\text{Li}$ and ${}^7\text{Li}$. The ${}^6\text{Li}$ isotope has a large neutron absorption cross-section with about 940 barn, while the neutron absorption of ${}^7\text{Li}$ is only about 0.0454 barn. When the neutron is incident on the natural crystal, some of the neutrons are absorbed by the ${}^6\text{Li}$ isotope in the crystal without being scattered, which results in the inaccuracy of the result. Therefore,

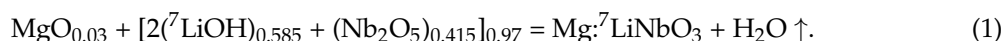
providing good crystals grown using only the ^7Li isotope in isolation has great significance for further investigation into the micro-structure of the LiNbO_3 crystal.

In our previous work, we reported on the studies on an undoped lithium isotope niobate ($^7\text{LiNbO}_3$) crystal [18]. Here, we mainly report on the specific crystal growth procedure, the determination of the crystal structure and crystal composition, and the characterization of the thermal properties, including specific heat, thermal expansion, thermal diffusion, and thermal conductivity, of Mg-doped lithium isotope niobate ($\text{Mg}:^7\text{LiNbO}_3$) single crystals.

2. Experimental Section

2.1. Crystal Growth Procedure

The conventional raw materials for growing LiNbO_3 crystals are Li_2CO_3 and Nb_2O_5 . However, due to the limited availability of isotopic materials, the starting materials for growing the $\text{Mg}:^7\text{LiNbO}_3$ crystal were $^7\text{LiOH}$ (with 99.9% chemical purity and 99.3% ^7Li isotopic purity), Nb_2O_5 (with 99.99% purity; Tianjin Institute of Pure Chemical Reagents, Tianjin, China), and MgO (with 99.99% purity; Tianjin Institute of Pure Chemical Reagents, Tianjin, China), which reacted as per the proportions described in Equation (1).



The chemical activity of $^7\text{LiOH}$ is strong, allowing it to easily absorb H_2O and CO_2 from the air to form $^7\text{LiOH}\cdot\text{H}_2\text{O}$ and $^7\text{Li}_2\text{CO}_3$. In addition, $^7\text{LiOH}$ is strongly alkaline and can easily corrode the platinum crucible, especially at high temperatures. Therefore, the preparation technique of isotopic crystals from $^7\text{LiOH}$ and Nb_2O_5 was expected to be much harder than that for the natural crystal from Li_2CO_3 and Nb_2O_5 raw materials. The specific preparation procedure is described below.

Initially, $\text{Mg}:^7\text{LiNbO}_3$ polycrystalline materials were prepared. Firstly, $^7\text{LiOH}$ was baked at about $100\text{ }^\circ\text{C}$ for at least 24 h to remove water, with the results showing that $^7\text{LiOH}$ lost up to 45% of its weight. Secondly, $^7\text{LiOH}$ was ground and combined completely with MgO and Nb_2O_5 according to the stoichiometric value, before the mixture was put into a platinum crucible, where a pure Nb_2O_5 pellet was placed at the bottom of the mixture to prevent contact between $^7\text{LiOH}$ and the crucible. Then, the crucible was heated to $450\text{ }^\circ\text{C}$ over 2 h and was kept stable for a further 2 h, before being heated to $900\text{ }^\circ\text{C}$ over 2 h and kept stable for a further 2 h. The crucible was finally heated to $1000\text{ }^\circ\text{C}$ over 2 h and kept stable for a further 5 h, after which the $\text{Mg}:^7\text{LiNbO}_3$ polycrystalline materials formed.

Subsequently, the $\text{Mg}:^7\text{LiNbO}_3$ crystal was grown using the Czochralski method in a TDL model-H50AC crystal-pulling apparatus. The apparatus used to heat the crucible was a 2-kHz low-radio-frequency furnace. Temperature control was achieved using a Eurotherm model 818 controller with a precision of $\pm 0.5\text{ }^\circ\text{C}$. The crawling distance of the pulling apparatus was less than $1\text{ }\mu\text{m}$. A *c*-axis natural LiNbO_3 crystal rod ($\Phi 2.8\text{ mm} \times 22\text{ mm}$) was used as the seed. During the growth process, the pulling rate ranged from 0.3 to 0.5 mm/h, and the rotation rate was kept at 5 rpm. After the growth was completed, the crystal was cooled to room temperature in air at a rate of $25\text{ }^\circ\text{C/h}$.

2.2. X-ray Powder Diffractometer (XPRD) Measurements

The phase identification of the as-grown crystal was determined using an X-ray powder diffractometer (XRPD; Bruker, model: Smart PPEX II) with a $\text{Cu K}_{\alpha 1}$ line ($\lambda = 1.5406 \times 10^{-10}\text{ m}$).

2.3. Crystal Composition Measurements

The crystal composition was determined using the Raman mode linewidth method. The Raman spectra were recorded on a Jobin-Yvon Model T64000 triple spectrometer with a spectral resolution of 2 cm^{-1} . Furthermore, a green 514.5-nm radiation from a Coherent Mode Innova 70 Ar^+ laser operating at 30 mW was employed for excitation of the spectra.

2.4. Transmittance Spectroscopy Measurements

The transmittance of the as-grown crystal was measured at room temperature using an infrared–visible–ultraviolet (IR–Vis–UV) spectrophotometer (Hitachi U-3500 model) in the range of 190–2500 nm, and the sample used was cut and polished with a thickness of 2 mm.

2.5. Thermal Property Measurements

The specific heat (C_p) was measured using a differential scanning calorimeter (Diamond DSC) with a simultaneous thermal analyzer made by the Perkin–Elmer company. A small sample weighing 23.20 mg was used for the measurements. Firstly, the sample was held at 298 K for 20 min, and was then heated to 573 K at a heating rate of 10 K·min^{−1}, before being held at 573 K for 20 min. The C_p value was calculated using the supplied software.

Thermal expansions of the as-grown crystal were measured, and the thermal expansion coefficients (α) were obtained using a thermal mechanical analyzer (TMA) made by the Perkin–Elmer company. The measurements were done along the crystallographic axis (expressed as X, Y, and Z) over a temperature range of 300 to 776 K with a heating rate of 5 K·min^{−1}. The measured sample was cut and polished with dimensions of 6 (X) × 6 (Y) × 4 (Z) mm³.

The thermal diffusion coefficients (λ) of the as-grown crystal were measured using a pulsed-laser method with a laser flash apparatus (Nanoflash LFA 447 nanoflash) in a temperature range of 301 to 572 K. Two square wafers with dimensions of 5 (X) × 5 (Y) × 1 (Z) mm³ and 5 (Y) × 5 (Z) × 1 (X) mm³ were coated with graphite on opposite faces, and the obtained values were calculated using the software supplied.

3. Results and Discussion

Figure 1 shows a photograph of the as-grown Mg:⁷LiNbO₃ single crystal along the *c* direction. Its dimensions were about Φ 20 mm × 20 mm, and its mass was about 40 g. It was transparent and free of inclusions as observed by the naked eye. Its color was a little darker than our previous undoped ⁷LiNbO₃ single crystal [18].



Figure 1. Photograph of the as-grown Mg:⁷LiNbO₃ crystal.

Figure 2 shows the XRPD results of the as-grown Mg:⁷LiNbO₃ crystal, which indicate that the as-grown Mg:⁷LiNbO₃ crystal exhibited the same crystal structure as that of natural LiNbO₃, whereby both belong to the hexagonal, 3-m point group and the R_{3c} space group. There were three molecules per unit cell ($Z = 3$). According to the peak 2θ values in the XRPD pattern, the unit-cell parameters were $a = b = 5.0857 \text{ \AA}$, and $c = 13.8405 \text{ \AA}$.

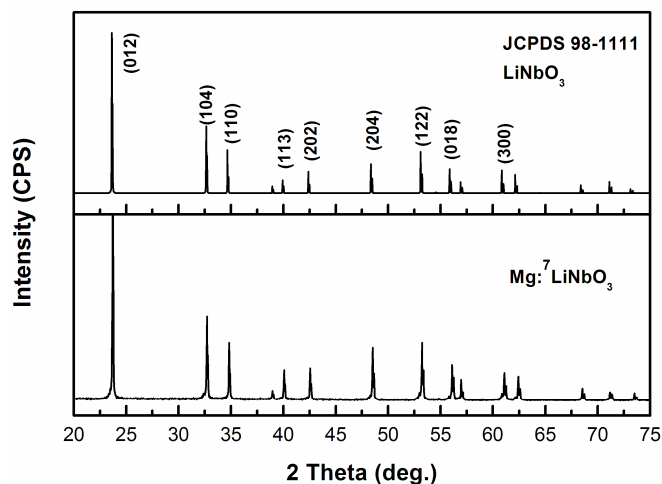


Figure 2. X-ray powder diffractometer (XRPD) pattern of the Mg:⁷LiNbO₃ crystal.

According to Equation (2) in Reference [19], the crystal composition of the LiNbO₃ crystal (Li% = the sum of ⁶Li and ⁷Li) can be estimated using the Raman mode linewidth (Γ) of the value of $E(\text{TO}_1)$ expected in the $x(\text{yz})x$ configuration.

$$[\text{Li}](\text{mol } \%) = 53.03 - 0.4739\Gamma. \quad (2)$$

For the Mg-doped ⁷LiNbO₃ crystal, the Li% (the sum of ⁶Li and ⁷Li, whereby the ⁶Li content is very small due to the original isotopic purity) can also be calculated using the same formula [19]. The obtained Raman spectrum at room temperature is plotted in Figure 3, and seven obvious $E(\text{TO})$ modes were observed. We could unambiguously identify that the $E(\text{TO}_1)$ mode was located at 157 cm^{-1} , and its linewidth was 8 cm^{-1} , obtained using the Peakfit software. From Equation (2) and the data obtained, we calculated the Li% as 49.29%.

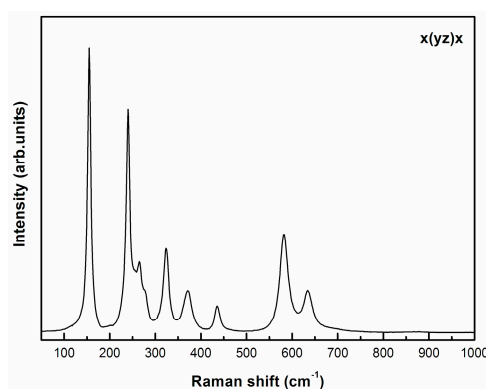


Figure 3. Room-temperature Raman spectrum of the Mg:⁷LiNbO₃ crystal recorded in the $x(\text{yz})x$ configuration.

The transmittance spectrum of the as-grown crystal is plotted in Figure 4, where we found that the crystal exhibited large transmittance, and the average value was approximately 72% in a wavenumber range of 500–2500 nm.

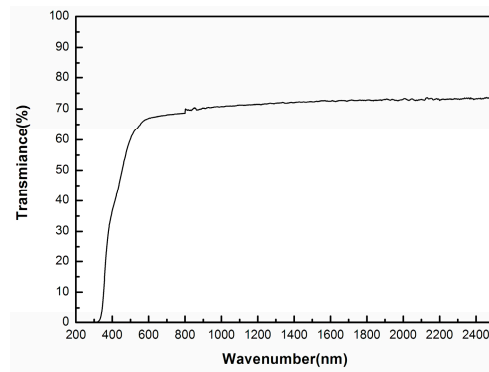


Figure 4. Transmittance spectrum of the Mg:⁷LiNbO₃ crystal.

The specific heat (C_p) is the ratio of the change in energy to the change in temperature, and it is the most important factor that influences the damage threshold of crystal materials [20]. Figure 5 shows the specific heat (C_p) curve of the as-grown Mg:⁷LiNbO₃ crystal. From the curve, it can be seen that the specific heat of the Mg:⁷LiNbO₃ crystal was almost linear with temperature, and it increased smoothly from $0.63 \text{ Jg}^{-1}\text{K}^{-1}$ to $0.85 \text{ Jg}^{-1}\text{K}^{-1}$ in the measured temperature range of 293 to 573 K, whereas it was $0.67 \text{ Jg}^{-1}\text{K}^{-1}$ at 328 K. The larger specific heat potentially makes it more useful for applications at high temperatures.

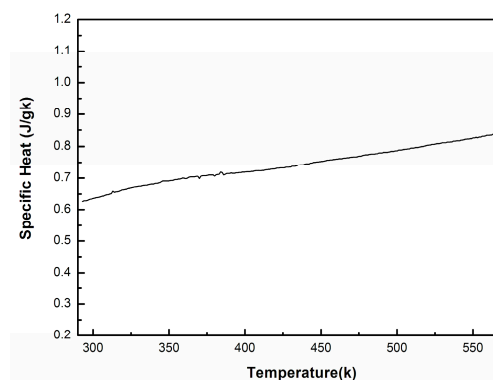


Figure 5. Specific heat curve of the Mg:⁷LiNbO₃ crystal.

The thermal expansion coefficient (α) is another important thermal parameter that affects the fracture of crystal materials [20]. The thermal expansion coefficient (α_{ij}) is a second-rank tensor [21], and the quadric representation of α_{ij} for the principle axis is shown in Equation (3).

$$\alpha_{11}x_1^2 + \alpha_{22}x_2^2 + \alpha_{33}x_3^2 = 1 \quad (3)$$

Correspondingly, in the principle coordinate system the α_{ij} tensor is diagonal, as shown in Equation (4), where α_{11} , α_{22} , and α_{33} represent the principle components of the thermal expansion coefficient tensor.

$$\begin{pmatrix} \alpha_{11} & 0 & 0 \\ 0 & \alpha_{22} & 0 \\ 0 & 0 & \alpha_{33} \end{pmatrix}. \quad (4)$$

As determined from the XRPD measurement, the Mg:⁷LiNbO₃ crystal belongs to the hexagonal and 3-m point group, where $\alpha_{11} = \alpha_{22}$. Therefore, the as-grown crystal exhibits only α_{11} or α_{22} and α_{33} as two independent principle components, as described in Equation (5), which can be obtained by measuring the thermal expansion along the X-axis (equivalent to a) and Z-axis (equivalent to c) of the crystal.

$$\begin{pmatrix} a_{11} & 0 & 0 \\ 0 & a_{11} & 0 \\ 0 & 0 & a_{33} \end{pmatrix}. \quad (5)$$

Figure 6 shows the thermal expansions ratio curves along the a -axis and c -axis of the as-grown $\text{Mg}^{7}\text{LiNbO}_3$ crystal, where the thermal expansion along the a -axis increased almost linearly in the measured temperature range, while the thermal expansion along the c -axis was different, as observed by the change in its slope at about 550 K.

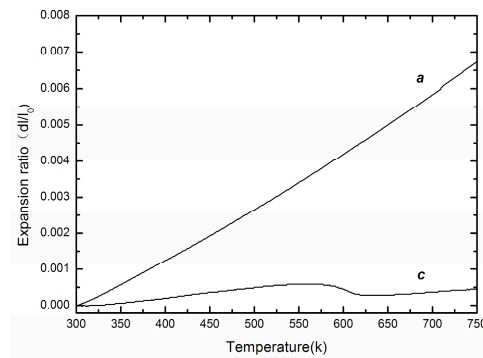


Figure 6. Thermal expansion curves along the a -axis and c -axis of the $\text{Mg}^{7}\text{LiNbO}_3$ crystal.

The thermal expansion coefficient can be calculated using Equation (6).

$$\bar{\alpha}(T_0 \rightarrow T) = \frac{\Delta L}{L_0} \frac{1}{\Delta T}, \quad (6)$$

where L_0 is the sample length at T_0 , ΔT is the temperature variation from T to T_0 , ΔL is the length change within ΔT , and $\bar{\alpha}$ is the average thermal coefficient over the temperature range from T to T_0 . Figure 7 shows the curves of the calculated thermal expansion coefficients versus the temperature along the a -axis and c -axis of the as-grown $\text{Mg}^{7}\text{LiNbO}_3$ crystal. From the curves, it can be seen that the $\text{Mg}^{7}\text{LiNbO}_3$ crystal only possessed positive thermal expansion when it was heated. Along the a -axis, the value increased steadily over the temperature range, while, along the c -axis, the value remained almost unchanged between 350 K and 550 K, before slightly decreasing to 640 K, after which it remained constant with rising temperature until 750 K. The calculated average thermal expansion coefficients were $\alpha_a = 13.2 \times 10^{-6} \text{ K}^{-1}$ and $\alpha_c = 1.5 \times 10^{-6} \text{ K}^{-1}$ from 300 K to 750 K. The value of the expansion coefficient along the a -axis was much larger than that along the c -axis, which shows that the as-grown crystal possessed large anisotropic thermal expansion, suggesting that the crystal grown along the c -axis could largely avoid internal pressure and fracture.

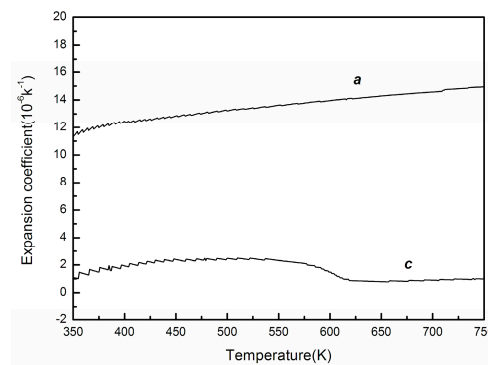


Figure 7. Thermal expansion coefficient curves along the a -axis and c -axis of the $\text{Mg}^{7}\text{LiNbO}_3$ crystal.

Thermal diffusion and thermal conductivity are also important factors for crystal materials from both a fundamental and an applied perspective. Both factors are also the symmetrical second-rank tensor. In our experiment, the thermal diffusion coefficients (λ) along the a -axis and c -axis were measured directly. Figure 8 shows the behavior of the thermal diffusion coefficient (λ) of the as-grown $\text{Mg}^{7}\text{LiNbO}_3$ crystal, which was anisotropic and decreased with increasing temperature. The thermal diffusion coefficient along the c -axis (λ_c) was slightly larger than that along the a -axis (λ_a). At 300 K, $\lambda_a = 1.75 \text{ mm}^2\text{s}^{-1}$ and $\lambda_c = 1.89 \text{ mm}^2\text{s}^{-1}$.

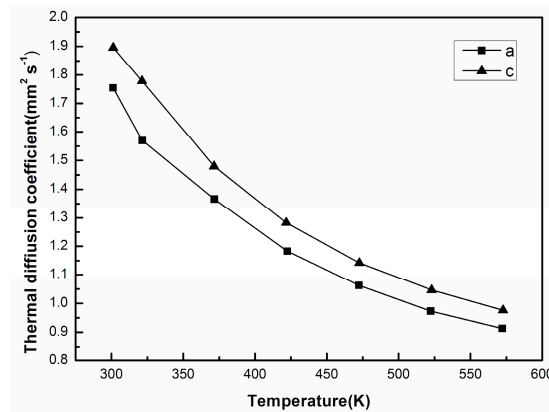


Figure 8. Thermal diffusion coefficient curve along the a -axis and c -axis of the $\text{Mg}^{7}\text{LiNbO}_3$ crystal.

The thermal conductivity (κ) can be calculated according to the following equation:

$$\kappa = \lambda\rho C_p, \quad (7)$$

where κ , λ , ρ , and C_p denote the thermal conductivity, thermal diffusion coefficient, density, and specific heat value at corresponding temperatures, respectively. The calculated thermal conductivities (κ) exhibited a similar tendency with thermal diffusion (λ), as shown in Figure 9, which decreased with rising temperature. In the temperature range of 301.1 K to 572.2 K, the thermal conductivity value along the a -axis decreased from $5.66 \text{ Wm}^{-1}\text{K}^{-1}$ to $3.47 \text{ Wm}^{-1}\text{K}^{-1}$, and the value along the c -axis decreased from $5.75 \text{ Wm}^{-1}\text{K}^{-1}$ to $3.49 \text{ Wm}^{-1}\text{K}^{-1}$.

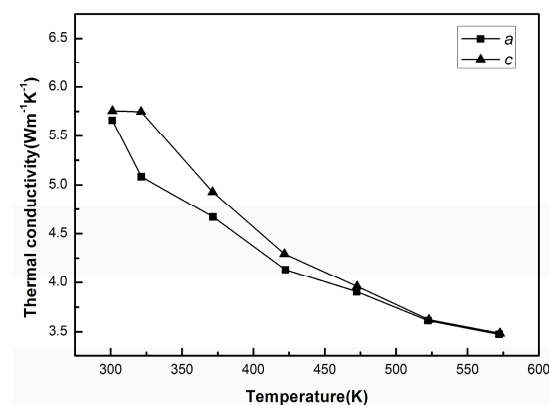


Figure 9. Thermal conductivity curves along the a -axis and c -axis of the $\text{Mg}^{7}\text{LiNbO}_3$ crystal.

All the measured thermal properties are listed in Table 1, where we also listed our previous results from the undoped $^7\text{LiNbO}_3$ crystals (including the congruent isotope lithium niobate, abbreviated as C^7LN , and the nearly stoichiometric isotope lithium niobate, abbreviated as NS^7LN), and results from the natural LiNbO_3 crystals (including the congruent lithium niobate, abbreviated as CLN , and the

nearly stoichiometric lithium niobate, abbreviated as NSLN). As shown in Table 1, we found that the specific heat (C_p) value of the as-grown $\text{Mg}^{77}\text{LiNbO}_3$ crystal was larger than that of C^{77}LN and CLN , but was smaller than that of NS^{77}LN and NSLN , which means that the grown $\text{Mg}^{77}\text{LiNbO}_3$ crystal exhibited a relatively moderate damage threshold [20]. The values of the thermal expansion coefficient (α) among the three isotope crystals were similar, which means that this thermal parameter was hardly affected by the intrinsic defects of the $^{77}\text{LiNbO}_3$ crystal, while both the values of the thermal diffusion coefficient (λ) and the thermal conductivity (κ) of the $\text{Mg}^{77}\text{LiNbO}_3$ crystal were larger than those of NS^{77}LN and NSLN , and even larger than those of C^{77}LN and CLN . Due to the relatively smaller quantity of ^6Li being substituted, the divergences in λ and κ were mainly a result of the defect micro-structure caused by the Li concentration (Li%).

According to Reference [22], κ can also be determined using the following equation:

$$\kappa = \rho C_p v L / 3, \quad (8)$$

where v is the constant sound velocity, and L is phonon mean free path (MFP). Phonon scattering in a solid consists of four processes involving collisions between phonons and (a) phonons, (b) defects, (c) free electrons, and (d) boundaries of the system [22]. A higher Li concentration results in a lower number of defects, since L (and κ) decreases with the increasing the number of defects. The collisions between phonons and defects explain why the thermal conductivity of C^{77}LN and CLN was smaller than that of $\text{Mg}^{77}\text{LiNbO}_3$, NS^{77}LN and NSLN . Because the doped Mg occupied the positions of Li or Nb sites in the crystal and made up for some vacancies [23], the as-grown $\text{Mg}^{77}\text{LiNbO}_3$ possessed the largest thermal conductivity among all the crystals.

Table 1. Experimental results of the as-grown $\text{Mg}^{77}\text{LiNbO}_3$ crystals in the present work and of the undoped $^{77}\text{LiNbO}_3$ crystals in our previous work [18], as well as of the natural LiNbO_3 crystals published by our team [6]. The values of specific heat (C_p) were determined at 328 K, the thermal diffusion coefficients (λ) and thermal conductivity (κ) were determined at 300 K, and the average thermal expansion coefficients (α) were obtained between 298 and 773 K. C^{77}LN —congruent isotope lithium niobate; NS^{77}LN —nearly stoichiometric isotope lithium niobate; CLN —congruent lithium niobate; NSLN —nearly stoichiometric lithium niobate.

Properties	Crystals				
	CLN	NSLN	C^{77}LN	NS^{77}LN	$\text{Mg}^{77}\text{LiNbO}_3$
Li%	48.53	49.74	47.34	49.72	49.29
C_p ($\text{Jg}^{-1}\text{K}^{-1}$)	0.60	0.70	0.62	0.76	0.67
α ($\times 10^{-6} \text{K}^{-1}$)	$\alpha_a = 16.1$	$\alpha_a = 17.2$	$\alpha_a = 13.2$	$\alpha_a = 13.5$	$\alpha_a = 13.2$
	$\alpha_c = 3.3$	$\alpha_c = 2.9$	$\alpha_c = 1.8$	$\alpha_c = 2.1$	$\alpha_c = 1.5$
λ (mm^2s^{-1})	$\lambda_a = 1.17$	$\lambda_a = 1.37$	$\lambda_a = 0.84$	$\lambda_a = 1.37$	$\lambda_a = 1.75$
	$\lambda_c = 1.26$	$\lambda_c = 1.62$	$\lambda_c = 1.10$	$\lambda_c = 1.62$	$\lambda_c = 1.89$
κ (W/mK)	$\kappa_a = 3.28$	$\kappa_a = 4.43$	$\kappa_a = 2.55$	$\kappa_a = 4.45$	$\kappa_a = 5.66$
	$\kappa_c = 3.54$	$\kappa_c = 5.23$	$\kappa_c = 3.10$	$\kappa_c = 5.25$	$\kappa_c = 5.75$
	Ref. [6]	Ref. [6]	Previous work	Previous work	Present work

4. Conclusions

Doped $\text{Mg}^{77}\text{LiNbO}_3$ crystals were successfully grown using the Czochralski method for a better investigation into the defect structure of the LiNbO_3 crystal. The as-grown crystal with a 49.29% Li concentration possessed the same structure as the natural LiNbO_3 crystal. The specific heat (C_p) increased slightly with temperature, and at 328 K, it was $0.67 \text{Jg}^{-1}\text{K}^{-1}$. The crystal exhibited positive thermal expansion behavior along both the a -axis and c -axis over the temperature range of 350 K to 750 K, and the calculated average thermal expansion coefficients (α) were $\alpha_a = 13.2 \times 10^{-6} \text{K}^{-1}$ and $\alpha_c = 1.5 \times 10^{-6} \text{K}^{-1}$. Both the measured thermal diffusion coefficient (λ) and the calculated thermal

conductivity (κ) decreased with rising temperature, and at 300 K, they were $\lambda_a = 1.75 \text{ mm}^2\text{s}^{-1}$ and $\lambda_c = 1.89 \text{ mm}^2\text{s}^{-1}$, and $\kappa_a = 5.66 \text{ Wm}^{-1}\text{K}^{-1}$ and $\kappa_c = 5.75 \text{ Wm}^{-1}\text{K}^{-1}$, respectively.

Author Contributions: Conceptualization, N.N. Zhang and J.Y. Wang. Formal analysis, M.J. Song. Investigation, X.R. Pan and X.S. Tai. Writing-Original Draft, N.N. Zhang. Writing-Review and Editing, N.N. Zhang and J.Y. Wang.

Funding: Natural Science Foundation of Shandong Province (BS2015CL012).

Acknowledgments: We gratefully thank the financial support of the National Natural Science Foundation (51372139), and the Higher Education and Technology Development Plan of Shandong Province (J15LA09).

Conflicts of Interest: The authors declare no conflict of interest.

References

1. Carruthers, J.R.; Peterson, G.E.; Grasso, M. Nonstoichiometry and crystal growth of lithium niobite. *J. Appl. Phys.* **1971**, *42*, 1846–1851. [[CrossRef](#)]
2. Imlau, M.; Badorreck, H.; Merschjann, C. Optical nonlinearities of small polarons in lithium niobate. *Appl. Phys. Rev.* **2015**, *2*, 040606. [[CrossRef](#)]
3. Arizmendi, L. Photonic applications of lithium niobate crystals. *Phys. Status Solidi (a)* **2004**, *201*, 253–255. [[CrossRef](#)]
4. Lim, H.H.; Prakash, O.; Joo, K.B.; Pandiyan, K.; Cha, M.; Rhee, B.K. Ultra-broadband optical parametric generation and simultaneous RGB generation in periodically poled lithium niobate. *Opt. Express* **2007**, *15*, 18294. [[CrossRef](#)] [[PubMed](#)]
5. Yu, E.N.; Choi, J.W.; Kang, H.; Ko, D.-K.; Fu, S.-H.; Liou, J.-W.; Kung, H.; Choi, H.J.; Kim, B.J.; Cha, M.; et al. Speckle noise reduction on a laser projection display via a broadband green light source. *Opt. Express* **2014**, *22*, 3547–3549. [[CrossRef](#)] [[PubMed](#)]
6. Yao, S.H.; Wang, J.Y.; Liu, H.; Hu, X.B.; Zhang, H.J.; Cheng, X.F.; Ling, Z.C. Growth, optical and thermal properties of near-stoichiometric LiNbO₃ single crystal. *J. Alloys Compd.* **2008**, *455*, 501–505. [[CrossRef](#)]
7. Wilkinson, A.P.; Cheetham, A.K.; Jarman, R.H. The defect structure of congruently melting lithium niobate. *J. Appl. Phys.* **1993**, *74*, 3080–3083. [[CrossRef](#)]
8. Grabmaier, B.C.; Otto, F. Growth and investigation of MgO-doped LiNbO₃. *J. Cryst. Growth* **1986**, *79*, 682–688. [[CrossRef](#)]
9. Grabmaier, B.C.; Wersing, W.; Koestler, W. Properties of undoped and MgO-doped LiNbO₃; correlation to the defect structure. *J. Cryst. Growth* **1991**, *110*, 339–347. [[CrossRef](#)]
10. Abdi, T.; Aillerie, M.; Fontana, M.; Bourson, P.; Volk, T.; Maximov, B.; Sulyanov, S.; Rubinina, N. Influence of Zn doping on electrooptical properties and structure parameters of LiNbO₃. *Appl. Phys. B* **1999**, *68*, 795–799. [[CrossRef](#)]
11. Sulyanov, S.; Maximov, B.; Volk, T.; Boysen, H.; Schneider, J.; Rubinina, N.; Hansen, T. Neutron and X-ray study of stoichiometric and doped LiNbO₃:Zn_{0.08}. *Appl. Phys. A* **2002**, *74*, S1031–S1033. [[CrossRef](#)]
12. Schirmer, O.F.; Thiemann, O.; Wohlecke, M. Defects in LiNbO₃—I. Experimental aspects. *J. Phys. Chem. Solids* **1991**, *52*, 185–200. [[CrossRef](#)]
13. Xu, H.; Lee, D.; He, J.; Sinnott, S.B.; Gopalan, V.; Dierolf, V.; Phillpot, S.R. Stability of intrinsic defects and defect clusters in LiNbO₃ from density functional theory calculations. *Phys. Rev. B* **2008**, *78*, 174103. [[CrossRef](#)]
14. Rajeev, B.; Indranil, B.; Sarveswaran, G.; Riscob, B.; Mohammad, S.; Ashwani, K.K.; Pradeep, K.G. Control of intrinsic defects in lithium niobate single crystal for optoelectronic applications. *Crystals* **2017**, *7*, 23–42.
15. Chia, C.-T.; Lee, C.-C.; Chang, P.-J.; Hu, M.-L.; Hu, L.J. Substitution mechanism of ZnO-doped lithium niobate crystal determined by powder X-ray diffraction and coercive field. *Appl. Phys. Lett.* **2005**, *86*, 182901. [[CrossRef](#)]
16. Argiolas, N.; Bazzan, M.; Ciampolillo, M.V.; Pozzobon, P.; Sada, C.; Saoner, L.; Zaltron, A.M.; Bacci, L.; Minzioni, P.; Nava, G.; et al. Structural and optical properties of zirconium doped lithium niobate crystals. *J. Appl. Phys.* **2010**, *108*, 093508. [[CrossRef](#)]
17. Serguei, S.; Tatyana, V. Lattice parameters of optical damage resistant in-doped LiNbO₃ crystals. *Crystals* **2018**, *8*, 210–216.

18. Zhang, N.N.; Wang, J.Y.; Yao, S.H.; Hu, X.B.; Zhang, H.J.; Ayala, A.P.; Guedes, I. Growth and characterization of congruent of lithium isotope niobate (${}^7\text{LiNbO}_3$) single crystal. *J. Cryst. Growth* **2011**, *318*, 645–648. [[CrossRef](#)]
19. Wohlecke, M.; Corradi, G.; Betzler, K. Optical methods to characterise the composition and homogeneity of lithium niobate single crystals. *Appl. Phys. B* **1996**, *63*, 323–330. [[CrossRef](#)]
20. Xu, D.; Zhang, K.C.; Zhang, L.H. *Science and Technology of Crystal Growth*; Science: Beijing, China, 1997.
21. Nye, J.F. *Physical Properties of Crystals*; Oxford University Press: Oxford, UK, 1985.
22. Choi, S.H.; Maruyama, S.; Kim, K.K.; Lee, J.H. Evaluation of the phonon mean free path in thin film by using classical molecular dynamic. *J. Korean Phys. Soc.* **2003**, *43*, 747–753. [[CrossRef](#)]
23. Abdi, F.; Aillerie, M.; Bourson, P.; Fontana, M.D. Defect structure in Mg-doped LiNbO_3 : revisited study. *J. Appl. Phys.* **2009**, *106*, 033519. [[CrossRef](#)]



© 2018 by the authors. Licensee MDPI, Basel, Switzerland. This article is an open access article distributed under the terms and conditions of the Creative Commons Attribution (CC BY) license (<http://creativecommons.org/licenses/by/4.0/>).